ChemPubSoc Europe

DOI: 10.1002/batt.201900176

BATTERIES & SUPERCAPS
Articles

Lithium Molybdate (Li_2MoO_3)–Sulfur Battery

Ruchira R. Dharmasena,[a, b] Alejandro Martinez-Garcia,[b, c, d] Veerendra Atla,[b, c] Muhammad Z. Akram,[b] Gamini U. Sumanasekera,[a, b] and Mahendra K. Sunkara*[b, c]

Here, we present a lithiated molybdate-sulfur battery with practical energy density greater than 300 Wh kg^{-1}. Electrochemically pre-lithiated α-MoO_3 is prepared to form lithium molybdate anode which was tested against mesoporous titania coated sulfur cathode. A pouch cell with a capacity of 5 mAh made using pre-lithiated lithium molybdate nanowires as anode and mesoporous TiO_2 (titania) coated carbon-sulfur cathode exhibited 1.4 V operating voltage and exhibited 620 Wh kg^{-1} capacity in the first cycle, dropped to ~400 Wh kg^{-1} in 2nd cycle and 300 Wh kg^{-1} at 100th cycle. Various prelithiation studies indicate that electrochemical lithiation of MoO_3 nanomaterials is crucial to make Li_2MoO_3 material suitable as anode. In situ electrochemical lithiation of MoO_3 anode is introduced as a method to fabricate lithium molybdate (Li_2MoO_3)-sulfur pouch cells in one step.

1. Introduction

Li-air battery (theoretical gravimetric capacity ~3623 Wh kg^{-1})[1] and lithium-sulfur (Li–S) battery (theoretical capacity of 1672 mAh g^{-1})[2] are of large interest toward energy storage for both electric vehicle and stationary applications. But, fabrication of a high capacity sulfur cathode for Li–S battery has always been challenging due to several reasons such as polysulfide dissolution in the ionic electrolytes,[3–4] polysulfide shuttling,[5–6] and high self-discharge.[7] When sulfur electrodes are tested against lithium metal as the anode (half-cell), the electrochemical performance suffers from lithium metal related phenomena such as dendrite formation[8] and SEI layer formation.[9] Graphite is obviously not a good host anode material for Li–S batteries due to its low gravimetric capacity,[10] yet there are some works done elsewhere using graphite anode with sulfur cathode to make lithium metal free Li–S full cells. Ref. [11] discusses the use of fluorinated ether to improve the performance of a pre-lithiated graphite-sulfur battery, giving 1000 mAh g^{-1} in the first cycle. A super concentrated ether electrolyte with pre-lithiated graphite anode and sulfur cathode has been investigated in Ref. [12]. They have demonstrated 686 mAh g$^{-1}_{(sulfur)}$ over 100 cycles. On the contrary, Si and Sn have very high specific capacity of 3570 mAh g^{-1}[10] and 991 mAh g^{-1} respectively. However, both the Si and Sn are known for their high-volume expansion upon lithiation; Si expands about 400% and Sn expands by >250%. These volume expansion causes pulverization and cracking[13–14] of the electrode. However, it has been shown that nanosized silicon particles intimately incorporated with Si can accommodate and withstand the volume expansion of silicon. Also, silicon nanowire architecture has shown promise as an anode material[15] and in[8] Si microfiber is used to prevent Li-dendrite formation in Li–S full cell. In addition Ref. [16], use of optimized Si microwire is discussed to minimize the capacity fade in Li ion batteries. High cyclability Li–S battery with pre-lithiated Si/SiO_2 nanosphere anode with 750 mAh g^{-1} over 500 cycle has been investigated in Ref. [17]. The expansion and chemical degradation with tin oxide was addressed through decoration of tin oxide nanowires with tin nanoparticles.[18] In addition Sn mixed with Graphene as an anode material to make Li–S full cell is discussed in Ref. [19].

MoO_3 nanowires were shown to be a stable anode material with intercalation potential between that of Si and graphite. MoO_3 material has recently attracted attention due to the existence of layered structure in one of its phases (α-MoO_3). Lithiated molybdenum oxide with small amount of Si has been shown to perform as an anode[20] with high capacity around 1043 mAh g^{-1} (10 A g^{-1}) over 50 cycles. There are few other reported works showing MoO_3 as an anode material for Li-ion batteries. Ref. [21] reports, single wall carbon nanotubes bridged MoO_3 with a half cell gravimetric capacity of 865 mAh g^{-1} (100 mA g^{-1}) at 100th cycle. In addition, Ref. [22] has reported a carbon free strategy using mixed Molybdenum oxides (MoO_x, $2<x<3$) to make anode material for Li-ion batteries with a half cell gravimetric capacity of 930.6 mAh g^{-1} (200 mA g^{-1}) at 200th cycle. Compared to these reports, $Li_{1.33}Mo_{0.66}O_2$ reported by our group in[20] performs better. Such discharging capacity as an anode material is a good match for

[a] Dr. R. R. Dharmasena, Prof. G. U. Sumanasekera
Department of Physics and Astronomy,
102 Natural Science Building
University of Louisville
Louisville KY 40292, USA
[b] Dr. R. R. Dharmasena, Dr. A. Martinez-Garcia, Mr. V. Atla, Dr. M. Z. Akram, Prof. G. U. Sumanasekera, Prof. M. K. Sunkara
Conn Center for Renewable Energy Research,
University of Louisville
216 Eastern Parkway
Louisville, KY 40292, USA
E-mail: mahendra@louisville.edu
[c] Dr. A. Martinez-Garcia, Mr. V. Atla, Prof. M. K. Sunkara
Department of Chemical Engineering,
University of Louisville
Louisville, KY 40292, USA
[d] Dr. A. Martinez-Garcia
Present Address: Intel Corporation, Hillsboro, OR, USA

Supporting information for this article is available on the WWW under https://doi.org/10.1002/batt.201900176

sulfur cathode to be used in a Li–S full cell. α-MoO_3 has also been synthesized by other methods such as vapor transport[23] and aqueous solution processing using ($Na_2MoO_4.2H_2O$).[24] The low expansion of α-MoO_3 upon lithiation makes it more suitable than β-MoO_3 for Li–S full cell. Further, it eliminates any safety issue associated with the use of lithium metal anode. One of the major issues with MoO_3 is its poor electrical conductivity. The conductivity has been shown to be improved using carbon coating.[25] Even without carbon, vertical arrays of MoO_x nanowires have exhibited better cyclability.[26]

Several researches have attempted fabricating Li–S full cells containing silicon anodes using silicon nanowires mixed with carbon and decorated with gold particles[27] and using Si/C[28] with Li_2S–C cathode as the lithium source.[29] In each case, poor performances have been observed with continuous degradation of discharge capacity. The reason for such degradation is due to both the use of poorly encapsulated sulfur in the cathode and the degradation of Si upon continuous cycling.

Here, mesoporous titania coated sulfur cathode[30] is paired against pre-lithiated, α-MoO_3 anode. Studies were performed using α-MoO_3 flakes and nanowires made using hotwire CVD and various pre-lithiation directions. The investigation presented here is first of its kind using lithium molybdate-sulfur chemistry and could spur low cost, high energy density, fast charge applications utilizing pre-lithiated molybdate anode.

Experimental Section

Sulfur cathode and MoO_3 anode preparation

The sulfur cathode is prepared by coating a sulfur/activated carbon electrode with mesoporous TiO_2.[30] α-MoO_3 is synthesized using a hot wire CVD technique as described in.[20] The material was deposited on the inner wall of a quartz glass tube using a co-centric Mo wire. The synthesis process was carried out for about 72 hours to collect several tens of grams of MoO_3 in powder form. The resulting MoO_3 was analyzed by XRD and confirmed to be α-MoO_3. As described in Ref. [20], Si nanoparticles suspended in ethanol is added to α-MoO_3 in micro gram quantity (< 1% by wt). The use of a very small amount of Si nanoparticles was earlier shown to improve the reversibility of α-MoO_3 nanomaterials.[20] Then, 5 mg of Silicon decorated α-MoO_3 is mixed with 7 mg of teflonized carbon binder (mixture of Polytetrafluoroethylene (PTFE) and acetylene black). This enables easy processing of electrode material to form circular pellets (0.7 mm in diameter and 0.5 mm thick) which can be easily pressed on to a stainless-steel mesh (Alpha Aesar- 80 mesh) current collector fitting in CR2032 coin cells.

In the half-cell assembly, metallic Li acts as a reservoir for Li-ions, whereas in the full cell configuration, the lithiated anode materials is the only source of Li-ions (in addition to electrolyte). Therefore, capacity balancing is necessary to ensure the availability of active material during cycling. Simple calculation of such capacity matching of sulfur cathode and $Li_{1.33}Mo_{0.66}O_2$ anode yields that ~5 mg of α-MoO_3 is required with 2 mg of sulfur. First, α-MoO_3 and Lithium metal electrodes were assembled in the coin cell format in a dry argon glove box as the initial step towards the Li–S full cell fabrication process. The electrolyte used in this cell consists of 1:1 ratio of 1,2-Dimethoxyethane (DME Sigma Aldrich) and 1,3-Dioxialane (DOL Sigma Aldrich) and 1 M of Bis(trifluoromethanesulfonimide) lithium salt (LiTFSI) and 1% wt. of $LiNO_3$. The assembled coin cell was connected to a battery tester (Arbin-16 cannels) and α-MoO_3 was galvanostatically lithiated at C/10 current rate to form $Li_{1.33}Mo_{0.66}O_2$. In this electrochemical lithiation process, α-MoO_3 electrode functions as a cathode. After α-MoO_3 is fully lithiated, the coin cell was dis-assembled inside the glove box and $Li_{1.33}Mo_{0.66}O_2$ electrode was carefully assembled as the anode in a fresh coin cell against afore mentioned sulfur electrode with fresh electrolyte which is same as in the lithiation process. Then the new S–$Li_{1.33}Mo_{0.66}O_2$ full cell was connected to the battery tester to perform the galvanostatic electrochemical testing.

Pouch cell fabrication and material preparation

After preliminary investigation of S- $Li_{1.33}Mo_{0.66}O_2$ full cell in coin cell configuration, it was necessary to scale up the α-MoO_3 production to enable the fabrication of high energy Li–S cells. The amount of α-MoO_3 synthesized using hot wire CVD technique described above is very low (20 mg in 72 hours). In order to scale up the α-MoO_3 synthesis, a novel and cost-effective method was investigated. First, synthesis of pre-lithiated MoO_3 using solvo-thermal techniques was attempted, but only resulted in Li_2MoO_4, which for obvious reasons is not a good reversible anode material for Li–S full cell applications. A description of the solvothermal technique is included in the supporting material. Since Mo in Li_2MoO_4 is at its highest oxidation state (+6), when assembled against a sulfur electrode, it cannot be oxidized any further via delithiation and fails to generate any open circuit voltage. Further, it was found to be difficult to directly intercalate lithium into layered MoO_3 using chemical or solvo-thermal techniques.

It was necessary to synthesize α-MoO_3 in bulk quantity and develop a technique to assemble a Li–S full cell in a single step process, which eliminates the cumbersome process of dis-assembling the cell after initial lithiation and re-assembling as Li–S full cell. In order to synthesize α-MoO_3 in bulk quantity, Mo was oxidized by heating Mo powder at 500 °C in air for two hours. MoO_3 (white powder) mostly in Monoclinic phase produced after the oxidation in air was converted to Orthorhombic α-MoO_3 by heating in a flow of 40% H_2/Ar (50 sccm) at 150 °C. After 10 hours of processing the initial white power turned blue and the final product was found to be α-MoO_3 by XRD.

In order to assemble high energy Li–S cells, electrodes were assembled in a pouch cell configuration. The main goal of this Li–S prototype is to fabricate a lithium sulfur cell in a single step. In practice, direct synthesis of prelithiated α-MoO_3 was found to be difficult. When α-MoO_3 is electrochemically prelithiated, Li^+ intercalate between the α-MoO_3 layers. Therefore, it was necessary to adopt a special design as shown in Figure 1, to fabricate a Li–S full cell starting with α-MoO_3 (before lithiation) and sulfur cathode using a single step process. The schematic diagram in Figure 1 of the pouch cell shows (a) before lithiation of α-MoO_3 (b) after lithiation of α-MoO_3. Red dashed lines show the Polypropylene separator (25 μm) completely covering both electrodes. Middle inter layer marked in green color is the lithium foil supported on a copper mesh.

Both cathode (sulfur) and anode (α-MoO_3 prior to lithiation) were synthesized in the ambient environment and Aluminum and Nickel tabs were spot-welded to the cathode and anode respectively as the battery terminals.. The pouch was fabricated using laminated aluminum sheets (MTI corp.). When designing the pouch cell prototype, target capacity was pre-determined to be 5 mAh. Then, mass loading of the electrodes and pouch dimensions were determined according to the targeted capacity of the pouch cell. Pouch and electrodes were dried in vacuum at 80 °C and then

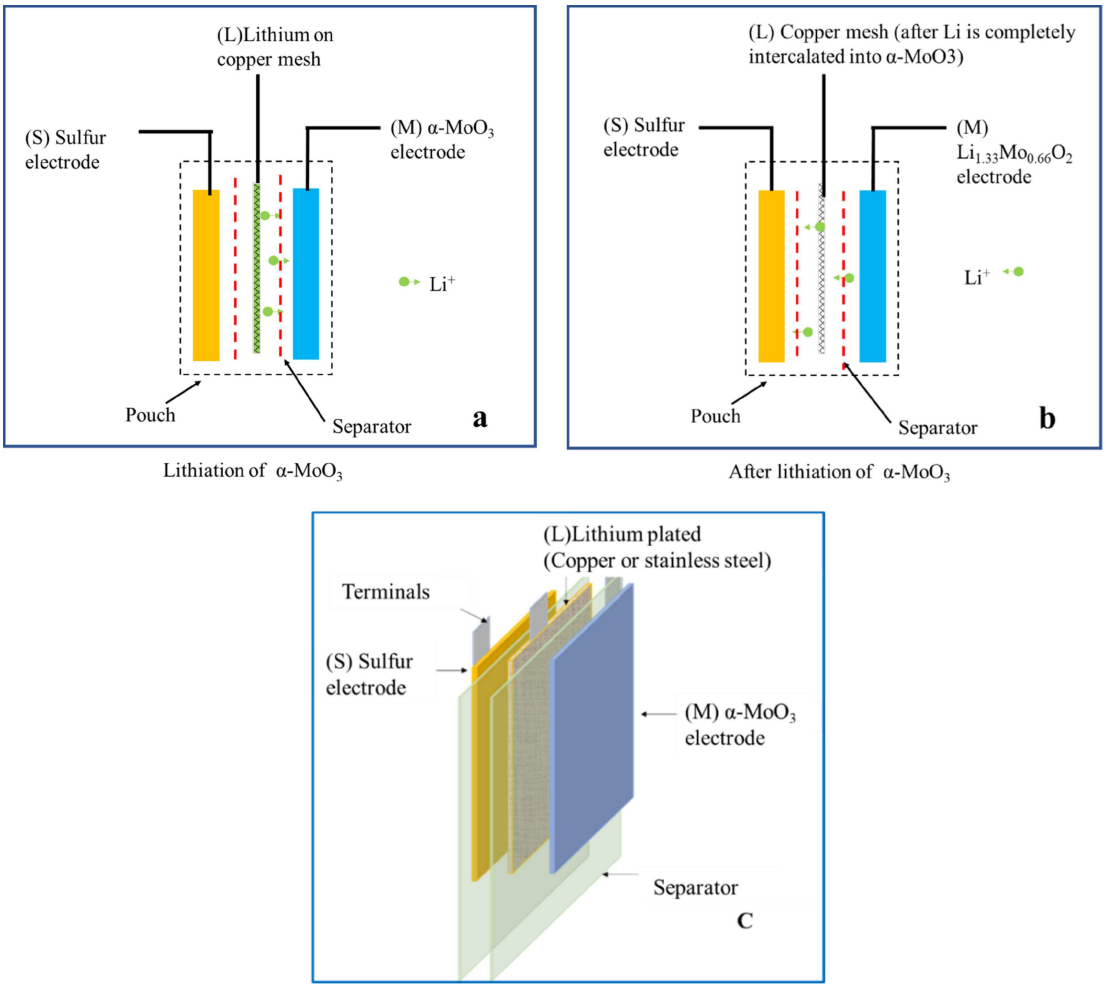

Figure 1. Schematic diagram of the pouch cell (a) before lithiation of α-MoO_3 (b) after lithiation of α-MoO_3. Red dashed lines show the separator completely covering both electrodes. Middle inter layer in green color is the lithium foil supported on copper mesh, (c) 3D sketch of the orientation of electrodes inside the pouch.

loaded into an Argon glove box for final assembling of the pouch cell. In this special pouch cell design, an additional thin lithium metal foil (80 μm), pressed on a copper gauze (80 mesh size) is sandwiched between the two electrodes which are already wrapped with the separator material to avoid electrical shorting. The Lithium foil serves as a sacrificial layer which is only utilized to lithiate the α-MoO_3 anode. High irreversible capacity 0.5 ml of electrolyte consisting of 1:1 ratio of 1,2-Dimethoxyethane (DME Sigma Aldrich) and 1,3-Dioxialane (DOL Sigma Aldrich) and 1 M of Bis(trifluoromethanesulfonimide) lithium salt (LiTFSI) and 1% wt. of $LiNO_3$ was filled. Pouch cell is then sealed using a pouch cell sealer inside the glove box. In this initial lithiation process, terminal "L" (Lithium metal) and the terminal "M" (α-MoO_3) are connected to the battery tester as the counter electrode and the working electrode respectively. After α-MoO_3 is fully lithiated, terminal "M" and terminal "S" (Sulfur) are connected to the battery tester as the counter electrode and the working electrode respectively for full cell cycling. When the full cell is designed, balancing of the electrodes masses is carefully done considering the sulfur cathode as the capacity limiting electrode.

Electrochemical and structural analysis

The full cells were cycled between 0.5 V and 2.8 V in galvanostatic mode using 16 channel Arbin battery test system. Cyclic voltammetry (CV) was performed at a scan rate of 0.3 mV/s in the range of 1.5 to 2.8 V (in a three electrode Swagelok cell configuration) using a biologic sp-200 electrochemical system. AC electrochemical impedance spectroscopy (EIS) of the cell utilizing three electrode configuration was used to investigate the same electrochemical system over the frequency range of 1 mHz to 1 MHz. All measurements were carried out at 25 °C.

Characterization

The morphology of the electrode surface was characterized by a TESCAN scanning electron microscope (SEM) and phase of materials using X-ray Diffractometer (Bruker D8).

2. Results and Discussion

Samples with α-MoO_3 directly deposited on stainless steel substrates using hot filament CVD were tested in half cell

configuration against Li in a coin cell. After full lithiation, the cell was disassembled and the binder free anode material ($Li_{1.33}Mo_{0.66}O_2$) was tested in a Li–S full cell against sulfur cathode. However, the capacity appears to degrade very quickly presumably due to delamination of anode material. In order to eliminate the delamination problem, α-MoO_3 is synthesized by Hot Wire CVD and scraped off the quartz reactor wall in a powder form and then mixed with carbon and binder. To confirm the electrochemical activity of Si decorated MoO_3 in carbon/binder matrix, in situ XRD test is carried while the α-MoO_3 is being lithiated. Figure 2 shows in situ XRD spectra during lithiation (including the spectrum of the as prepared material) of Hot Wire CVD deposited MoO_3 powder in teflonized acetylene black carbon binder electrode. The XRD results confirm that the pre-lithiation process in our sample is similar to that of directly deposited α-MoO_3 on stainless steel reported in.[20] The diffraction pattern of the as prepared Si@MoO_3 (red curve) is consistent with α-MoO_3 (JCPDS 00–005-0508) having an orthorhombic crystal structure and cell parameters $a = 3.962$ Å, $b = 13.858$ Å, $c = 3.697$ Å. The XRD spectra at the discharge voltages of 1.5 V, 1 V, and 0.2 V (black curves) show peaks corresponding to $Li_2Si_2O_5$ (004 and 111 reflections) and $Li_{1.33}Mo_{0.66}$ O_2 (311 and 400 reflections) (JCPDS 01-073-2300). As expected, 311 peak downshifts as the lithiation progresses implying increase of d spacing during lithiation.

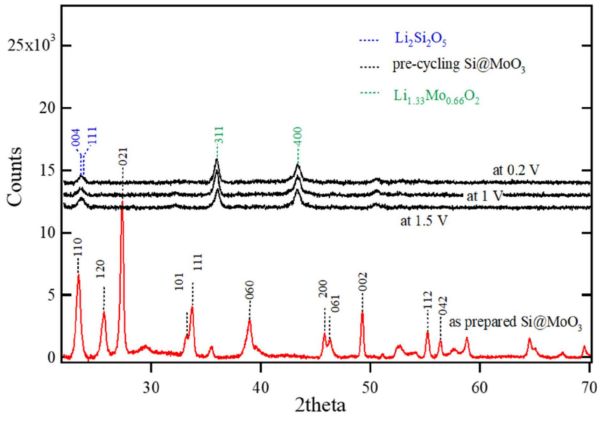

Figure 2. In situ XRD analysis for pre-lithiation of Hot Wire CVD deposited MoO_3 powder in teflonized acetylene black carbon binder electrode. α-MoO_3 [00-005-0508], $Li_{1.33}Mo_{0.66}O_2$ [01-073-2300] and $Li_2Si_2O_5$ [00-015-0637]

The discharge characteristics of the $Li_{1.33}Mo_{0.66}O_2$–S full cell assembled in a coin cell configuration are presented in Figures 3a and 3b during cycling at C/10 rate. Initial capacity of 905 mAh g^{-1} is seen to retain at 400 mAh g^{-1} (with respect to sulfur weight) after 50th cycle at C/10 rate. The full cell is designed in such a way that the capacity is limited by the cathode. The cell has an open cell potential of around 2.3 V. The IR drop of the voltage-capacity curve is higher compared to a Li -S half-cell. The specific capacity is seen to fade steadily with the cycle number. One reason could be due to electrode degradation in the anode leading to poor charge transference.

Figure 4a shows the cyclic voltammetry (CV) curve of $Li_{1.33}Mo_{0.66}O_2$–S full cell. Three electrode, Swagelok test cell (schematically shown in Figure 4b) was used for the CV by keeping lithium as the reference electrode, $Li_{1.33}Mo_{0.66}O_2$ anode as the counter and sulfur cathode as the working electrode. As can be seen from the CV curves shown in Figure 4a, the oxidation and reduction activity of the sulfur (working) electrode is similar to that of Li–S half-cell electrochemical activity.[30] The reduction peak at 2.4 V is known to occur when soluble Li_2S_8 forms. Further reduction of longer poly sulfide chains to shorter poly sulfide chains first forming soluble Li_2S_6 and Li_2S_4 and finally converting to solid forms of Li_2S_2 and Li_2S is represented by a second reduction peak at 1.9 V. The presence of oxidation peak at 2.5 V, confirms the reversibility of the $Li_{1.33}Mo_{0.66}O_2$–S full cell which requires enough Li ions (available from the counter electrode) during the cell cycling.

Finally, the electrochemical impedance analysis (EIS) was carried out in the same T-Swagelok cell, (schematically shown in Figure 4b) but with a platinum wire as the reference

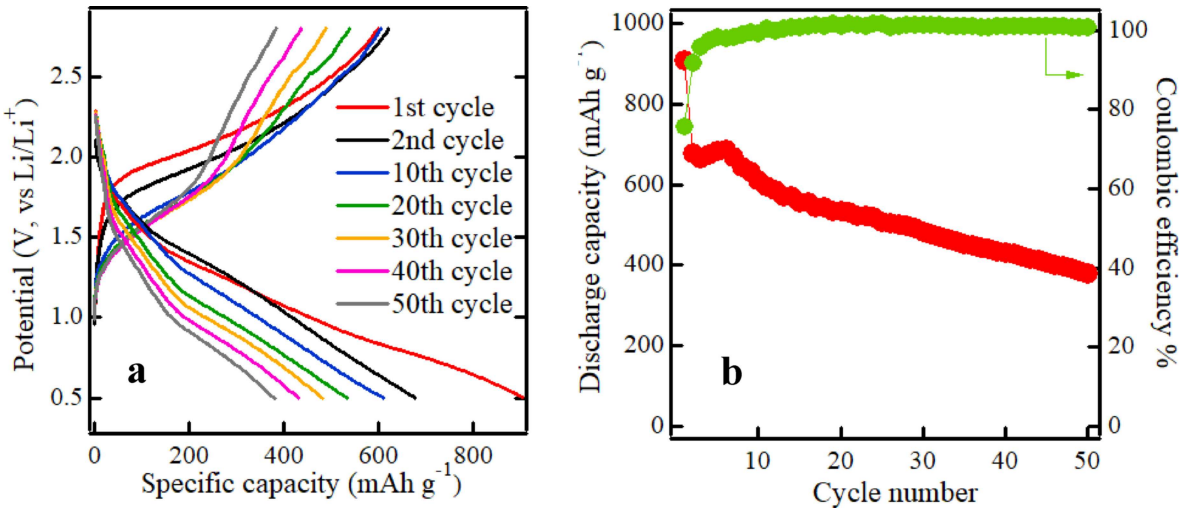

Figure 3. (a) Potential vs discharge curve of $Li_{1.33}$ $Mo_{0.66}O_2$–S full cell (b) capacity vs cycle number and coulomb efficiency of $Li_{1.33}Mo_{0.66}O_2$–S full cell at C/10 rate.

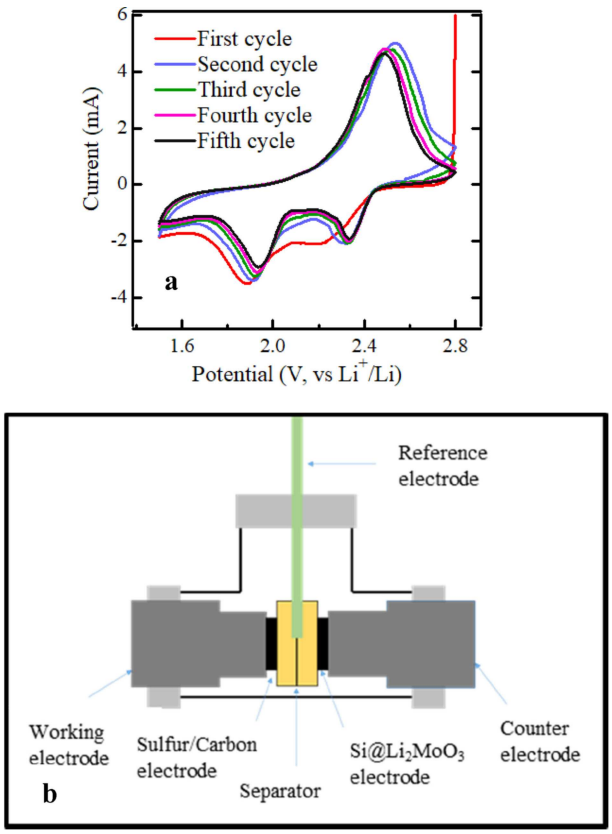

Figure 4. (a) Cyclic voltammetry curve of $Li_{1.33}Mo_{0.66}O_2$–S (working electrode vs reference electrode) (b) Schematic of three electrode Swagelok test cell which used for CV.

electrode. The sulfur electrode is used as the working electrode while $Li_{1.33}Mo_{0.66}O_2$ electrode is used as the counter electrode. For EIS studies, a platinum wire can be an effective reference electrode[31] with minimal influence on EIS data. Further, the reference electrode is positioned in the middle of two glass-fiber separators of equal thickness (1 mm). The impedance was measured in the A/C frequency range of 1 MHz to 1 mHz at potential values of 1 V, 0.7 V and 0.5 V and 0.2 V (100% DoD) during the discharge and at 1 V, 1.5 V, 2 V and 2.8 V (100% DoC) during the charging as shown in Figure S1a and S1b.

The Nyquist plots were obtained as shown in the Figure S2 in the supporting document. Nyquist plots were fitted using EIS fitting software (EC-LAB). A constant phase element and a resistor in parallel represent a semi-circle of Nyquist plots. Two convoluted semi-circles were identified in each Nyquist plot. Resistance values were identified for the electrolyte resistance (R_e), Charge transference resistance (R_{cct} (for cathode) and R_{act} (for anode)) and interface resistance (R_{int}) by fitting with appropriate network models. Tables 1 and 2 show the variation of fitted resistor values corresponding to DOD % and DOC %.

The increase of electrolyte resistance, R_e in the cathode (Table 1) from the initial value of 40 Ω up to about 70 Ω indicates that lithium polysulfides are formed at 100% discharge. As the electrochemical reaction progresses in the sulfur electrode, charge transfer resistance, R_{cct} decreases since electrically insulating elemental sulfur is converted into ionic Li_2S. In the same time, solid electrolyte interface on sulfur electrode, R_{int} increases from the initial value of 10 Ω to the final value of 30 Ω. This could be due to the solid Li_2S formation which could influence the electrode-electrolyte interactions. The electrolyte resistance R_e near anode electrode, however, shows a decrease by few ohms while the interface resistance rises on the anode. Charge transfer resistance of counter electrode, R_{act} at discharge however is comparatively stable.

Thus, we can assume that, $Li_{1.33}Mo_{0.66}O_2$ electrode integrity is intact while discharging. When the full cell is charged (as shown in Figure S3c in the supporting information), it is noticeable that, R_e near the sulfur electrode is decreased as the polysulfide concentration is lowered due to the oxidation of S^{-2} to S. Charge transference resistance R_{cct} is increased as the cathode accumulates sulfur introducing poor electronic conductivity of the cathode. It is an interesting phenomenon to observe that, R_{int} at cathode drops as the cell is re-charged which is the expected result when Li_2S dissociate to Li and S. Anode (Figure S3d) on the other hand shows an increase of R_e and R_{act}. This can be explained as due to the shuttling of any dissolved polysulfides towards the anode. Migration of dis-

Table 1. Summary of the impedance values obtained at various depth of discharge (DoD).

DOD %/ Resistance	4% cathode Ω	anode Ω	58% cathode Ω	anode Ω	80% cathode Ω	anode Ω	100% cathode Ω	anode Ω
R_e	41.2	55.1	48.2	49.9	55.5	46.7	72.2	41.2
R_{cct}/R_{act}	44.3	81.1	10.0	80.7	3.7	80.9	0.05	70.6
R_{int}	8.2	2.6	20.9	25.7	22.4	36.3	30.9	55.2

Table 2. Summary of the impedance values obtained at various depth of charge (DoC).

DOC %/ Resistance	6% cathode Ω	anode Ω	42% cathode Ω	anode Ω	70% cathode Ω	anode Ω	100% cathode Ω	anode Ω
R_e	40.9	40.4	41.8	40.5	38.0	48.6	31.7	82.4
R_{cct}/R_{act}	15.2	20.3	12.6	40.1	22.8	58.2	32.6	74.2
R_{int}	58.2	46.0	21.7	35.3	14.3	3.5	11.2	–

solved polysulfides is believed to increase the electrolyte resistance R_e. Increase of R_{act} could be due to the lattice expansion of $Li_{1.33}Mo_{0.66}O_2$ upon recharge, causing carbon and $Li_{1.33}Mo_{0.66}O_2$ contact loss.

Figure 5(a) and (b) show the SEM images of as prepared MoO_3 (by direct oxidation of Mo powder) and after reduction in a flow of Ar/H_2 respectively. The as prepared MoO_3 sample consists of planar platelets co-existing with other irregular particles smaller than 5 μm as seen in the SEM image in Figure 5(a). It appears that the initial oxidation of Mo results in mixed α/β-MoO_3 phases. After reduction in H_2/Ar, the morphology of the particles has been changed primarily to larger planar platelets of α-MoO_3 as evidenced by the SEM image in Figure 5b. Figure 5(c) shows the XRD spectra of MoO_3 sample before and after reduction. The XRD spectrum for the sample before reduction is consistent with α-MoO_3 (JCPDS 00-005-0508) having an orthorhombic crystal structure with cell parameters $a = 3.962$ Å, $b = 13.858$ Å, $c = 3.697$ Å and additional peaks located at $2\theta = 23.95°$ and 28.73° which were assigned to the characteristic reflections from (020) and (112) planes of β-MoO3 (JCPDS 01-084-1360), respectively. The XRD pattern for the sample after reduction mostly consists of α-MoO_3.

Figure S7b and S7d show the half-cell electrochemical performance of sulfur cathode (sulfur mixed with activated carbon and coated with mesoporous TiO_2)[30] and α-MoO_3 anode which made of α-MoO_3 particles. The cathode shows capacity as high as 900 mAh g^{-1} even after 100 cycles at C/3 rate, but the anode capacity fades to ~300 mAh g^{-1} after 50 cycles. Pristine sulfur cathode has a potential of 2.4 V and completely lithiated α-MoO_3 ($Li_{1.33}Mo_{0.66}O_2$) has a potential of ~0.2 V versus lithium. Therefore, a combination of these two electrodes will give an open circuit voltage of ~2.3 V.

Figure 6b and 6c show the performance of the pouch cell assembled from the respective cathode and anodes after initial lithiation process. The pouch cell has a gravimetric capacity of 1200 mAh g^{-1} at the first cycle and about 380 mAh g^{-1} at the 50th cycle and the cell is cycled at C/3 rate. Here, we believe that the capacity contribution of TiO_2 coating is negligible as the electrode contains only about 5% of titania compared to sulfur. In terms of the specific capacity, it is apparent that, the Li–S battery with sulfur/carbon cathode and α-MoO_3 anode in the proposed pouch cell design provide a specific capacity greater than that of available Li-ion technologies, but at a lower nominal potential ~1.4 V. The sulfur cathode used in this full

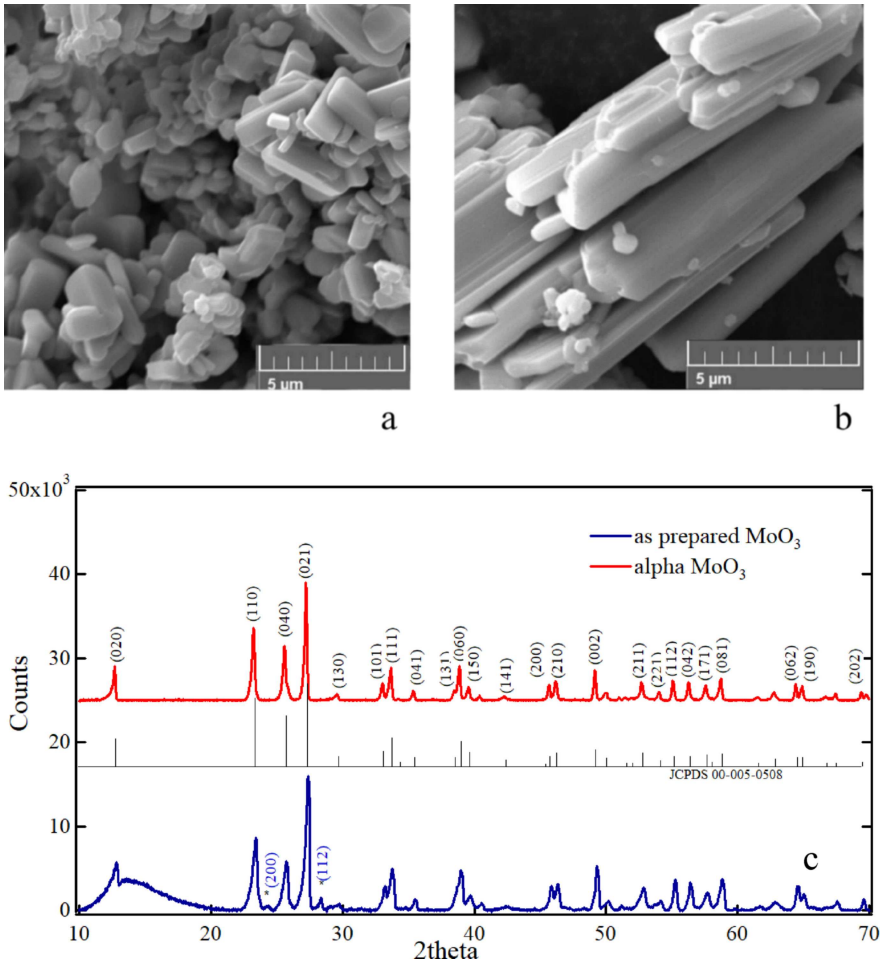

Figure 5. SEM images of (a) as prepared MoO_3 after oxidizing at 500 °C (b) α-MoO_3 after reduction in 40 % H_2/Ar at 150 °C (c) XRD spectrums of as prepared MoO_3 and α-MoO_3 after reduction in 40 % H_2/Ar.

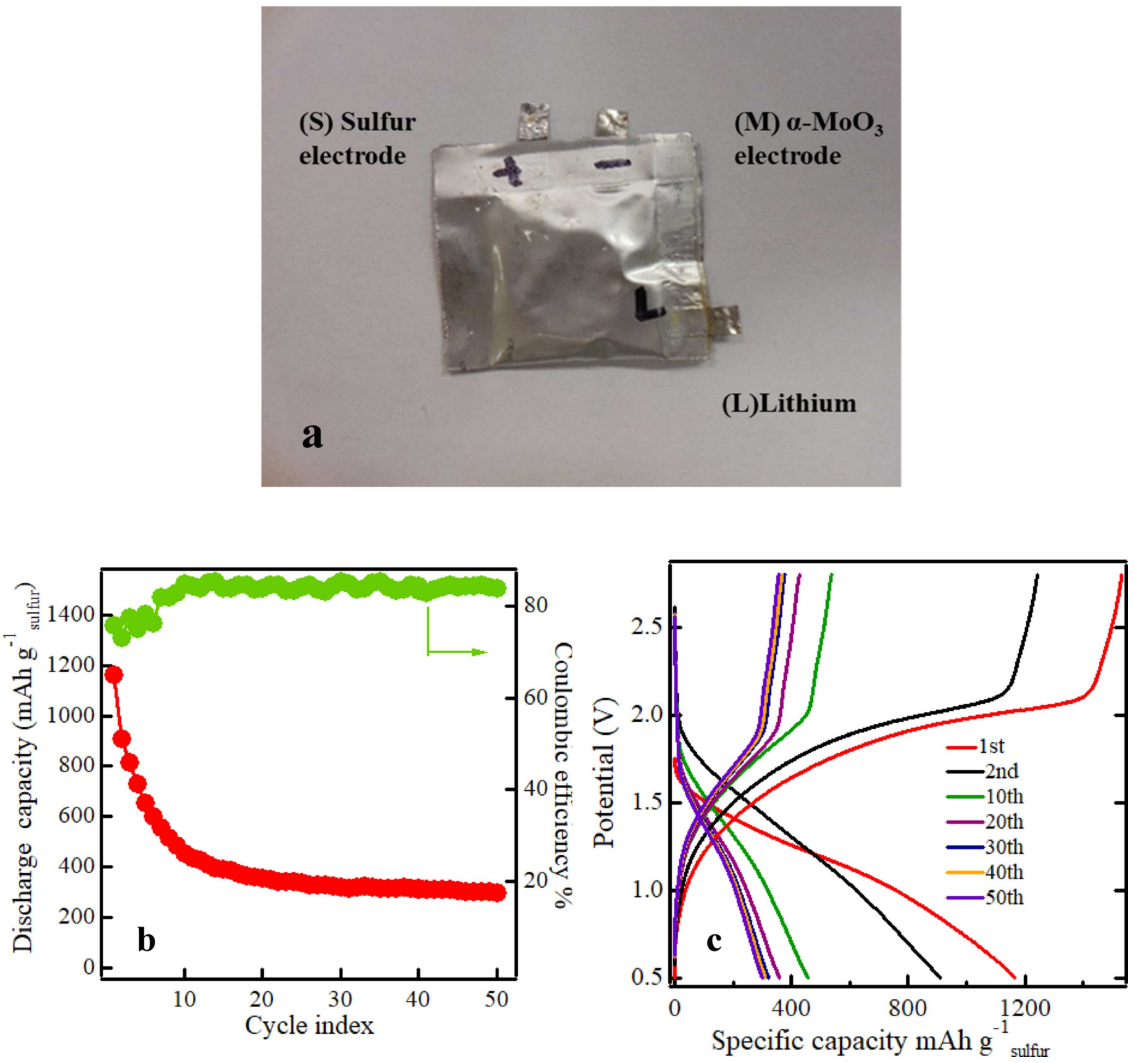

Figure 6. (a). Picture of a finished pouch cell (b). Discharge capacity vs cycle index (c) Potential vs specific capacity of S–$Li_{1.33}Mo_{0.66}O_2$

cell was developed by our group[30] showing a stable specific capacity over 900 mAh g^{-1} over 100 cycles. However, the specific capacity of the full cell was found to degrade from its high initial value and stabilize at 300 mAh g^{-1}. The reason for such capacity degradation could due to the performances of the $Li_{1.33}Mo_{0.66}O_2$ anode which tend to stabilize around 300 mAh g^{-1} as shown in Figure S4d.

The same pouch cell design was used to assemble high energy density pouch cells using α-MoO_3 nanowires. The α-MoO_3 nanowires were synthesized by hydrogenating the impure MoO_3 which was derived by solvothermal reaction of 5:1 wt% ratio of MoO_2 and KCl at 500 °C. The electrochemical characteristics of lithium molybdate nanowire half-cell are shown in Figure S4a and S4b. In contrast to the anodes made of α-MoO_3 micro particles, α-MoO_3 nanowires demonstrate a stable specific capacity of 400 mAh g^{-1} at C/10 rate. In addition, its delithiation potential ranges from 0.2 V to 1.5 V. In the reference,[20] binder free α-MoO_3 anode demonstrates superior discharge specific capacity giving ~1000 mAh g^{-1} vs lithium, but its mass loading is very low. We believe, that 400 mAh g^{-1} of nanowire based α-MoO_3 anode is due to its electrode pulverization. To gain a stable potential plateau around 1.5 V in lithium molybdate-sulfur pouch cell, mass balancing was done within the delithiation potential 0.2 V −1.0 V for the anode to compensate the practical 700 mAh g^{-1} capacity of the sulfur cathode. Figure S5 in the supporting document demonstrates the potential vs specific capacity curves of cathode and anode which are used to calculate the capacity matching and mass loading. Figure 7a shows the specific energy density data of lithium molybdate nanowire-sulfur full cell with a 3 mAh practical capacity (Figure S6). The mass loading of cathode and anode are 4.2 mg and 5.6 mg respectively. The assembled full cell demonstrates a promising 300 Wh kg^{-1} specific energy density after 100th cycle with a stable 1.4 V nominal potential as shown in Figure 7a and 7b. Figure 7c, shows the comparison of electrochemical characteristics of currently reported Li–S full cells made of : Si,[29] Sn[32] and graphite[33] together with the electrochemical characteristics of S–$Li_{1.33}Mo_{0.66}O_2$ full cell.

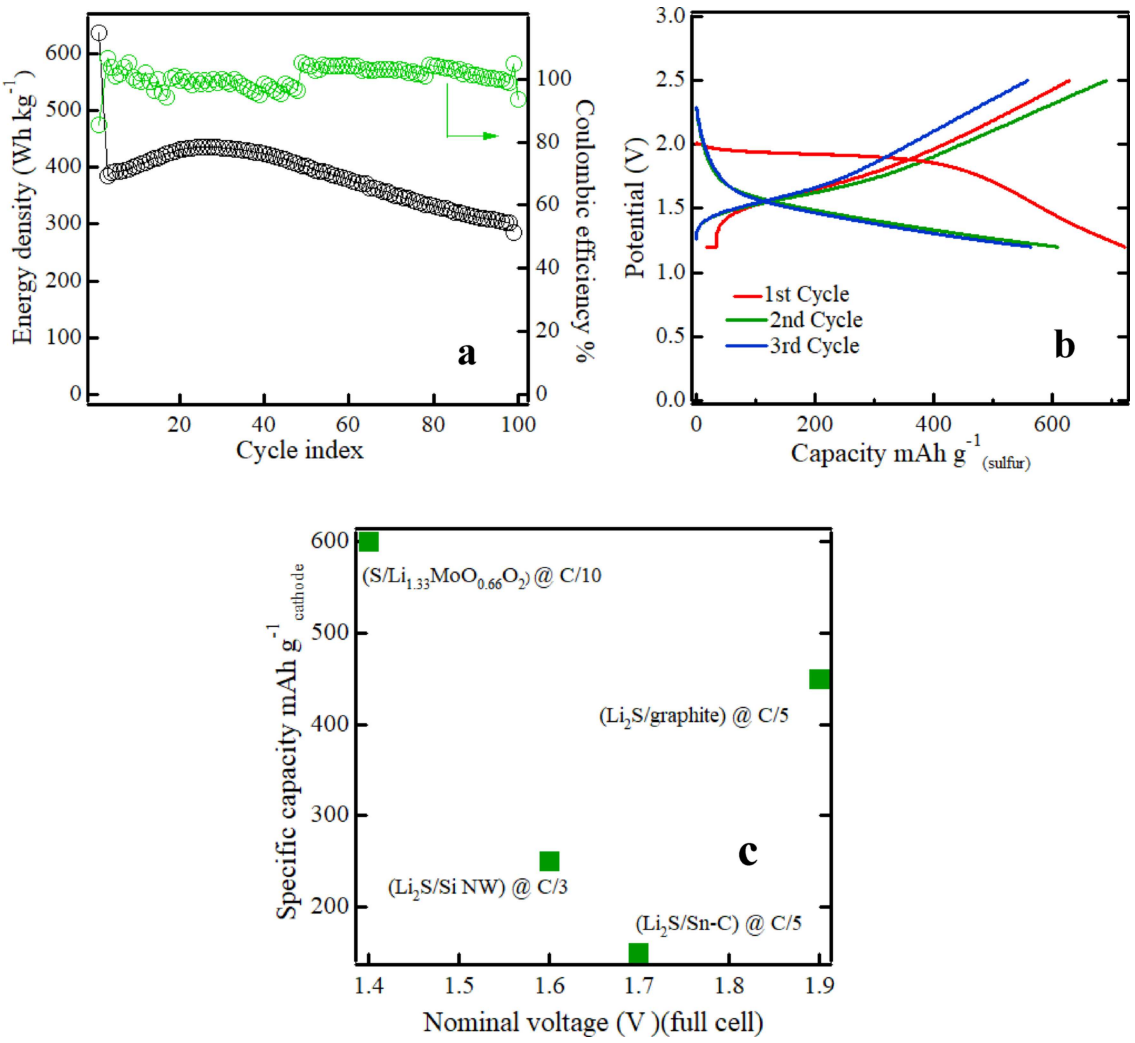

Figure 7. Electrochemical characteristics of lithium molybdate (nano-wire)-sulfur full cell (a) specific energy density curve (b) potential vs specific capacity curve (c) a comparison of Li-S full cell performances, made of Si, Sn, graphite anodes and $Li_{1.33}Mo_{0.66}O_2$ anode discussed in this work. Gravimetric capacity is based on cathode active material mass.

3. Conclusions

In this work, it has been shown that $Li_{1.33}Mo_{0.66}O_2$ is a potential candidate as an anode material in Li–S batteries. Cyclic voltammetry data of Li–S full cell indicate that redox reactions in the sulfur electrode are similar to that of sulfur electrode in Li–S half-cell indicating presence of sufficient lithium ion supply from the lithium molybdate anode. In addition, α-MoO_3 can be synthesized in high quantities using H_2 /Ar so that α-MoO_3 can be used in powder form to scale up the Li–S full cell fabrication. Further, it is found that, lithium molybdate for the Li–S full cell can only be made using intercalation, but not with chemical reactions.

Acknowledgements

Authors gratefully acknowledge the Conn Center for Renewable Energy Research for access to facilities and characterization equipment. This material is based upon work supported by I/UCRC Grant (1624712) and partially from National Science Foundation under co-operation agreement No 1355438.

Keywords: batteries · lithium molybdate · lithium sulfur · molybdenum oxide · polysulfides

[1] J. Lu, L. Li, J. B. Park, Y. K. Sun, F. Wu, K. Amine, *Chem. Rev.* **2014**, *114*, 5611–5640.
[2] A. Manthiram, Y. Fu, S. H. Chung, C. Zu, Y. S. Su, *Chem. Rev.* **2014**, *114*, 11751–11787.
[3] J. Scheers, S. Fantini, P. Johansson, *J. Power Sources* **2014**, *255*, 204–218.
[4] S. S. Zhang, *J. Power Sources* **2013**, *231*, 153–162.
[5] Y. Diao, K. Xie, S. Xiong, X. Hong, *J. Power Sources* **2013**, *235*, 181–186.
[6] Y. V. Mikhaylik, J. R. Akridge, *J. Electrochem. Soc.* **2004**, *151*, A1969.
[7] H. S. Ryu, H. J. Ahn, K. W. Kim, J. H. Ahn, K. K. Cho, T. H. Nam, *Electrochim. Acta* **2006**, *52*, 1563–1566.
[8] M. Hagen, E. Quiroga-González, S. Dörfler, G. Fahrer, J. Tübke, M. J. Hoffmann, H. Althues, R. Speck, M. Krampfert, S. Kaskel, *J. Power Sources* **2014**, *248*, 1058–1066.

[9] S. J. An, J. Li, C. Daniel, D. Mohanty, S. Nagpure, D. L. Wood, *Carbon* **2016**, *105*, 52–76.
[10] B. Liang, Y. Liu, Y. Xu, *J. Power Sources* **2014**, *267*, 469–490.
[11] S. Chen, Z. Yu, M. L. Gordin, R. Yi, J. Song, D. Wang, *ACS Appl. Mater. Interfaces* **2017**, *9*, 6959–6966.
[12] P. Zeng, Y. Han, X. Duan, G. Jia, L. Huang, Y. Chen, *Mater. Res. Bull.* **2017**, *95*, 61–70.
[13] U. Kasavajjula, C. Wang, A. J. Appleby, *J. Power Sources* **2007**, *163*, 1003–1039.
[14] J. Li, A. K. Dozier, Y. Li, F. Yang, Y.-T. Cheng, *J. Electrochem. Soc.* **2011**, *158*.
[15] C. K. Chan, H. Peng, G. Liu, K. MCilwrath, X. Feng Zhang, R. A. Huggins, Y. Cui, *Nat. Nanotechnol.* **2007**, *3*.
[16] E. Quiroga-González, J. Carstensen, H. Föll, *Electrochim. Acta* **2013**, *101*, 93–98.
[17] S. K. Lee, S. M. Oh, E. Park, B. Scrosati, J. Hassoun, M. S. Park, Y. J. Kim, H. Kim, I. Belharouak, Y. K. Sun, *Nano Lett.* **2015**, *15*, 2863–2868.
[18] C. P. Praveen Meduri, V. Kumar, G. U. Sumanasekera, M. K. Sunkara, *Nano Lett.* **2009**, *9*, 612–616.
[19] E. Hari Mohan, B. V. Sarada, R. Venkata Ram Naidu, G. Salian, A. K. Haridas, B. V. Appa Rao, T. N. Rao, *Electrochim. Acta* **2016**, *219*, 701–710.
[20] A. Martinez-Garcia, A. K. Thapa, R. Dharmadasa, T. Q. Nguyen, J. Jasinski, T. L. Druffel, M. K. Sunkara, *Sci. Rep.* **2015**, *5*, 10530.
[21] H. Sun, D. Hanlon, D. A. Dinh, J. B. Boland, A. E. Del Rio Castillo, C. Di Giovanni, A. Ansaldo, V. Pellegrini, J. N. Coleman, F. Bonaccorso, *2D Mater.* **2017**, *5*.
[22] D. Wu, R. Shen, R. Yang, W. Ji, M. Jiang, W. Ding, L. Peng, *Sci. Rep.* **2017**, *7*.
[23] F. C. Weiyang Li, Z. Tao, J. Chen, *J. Phys. Chem.* **2005**, *110*, 119–124.
[24] K. Sakaushi, J. Thomas, S. Kaskel, J. Eckert, *Chem. Mater.* **2013**, *25*, 2557–2563.
[25] M. F. Hassan, Z. P. Guo, Z. Chen, H. K. Liu, *J. Power Sources* **2010**, *195*, 2372–2376.
[26] P. Meduri, E. Clark, J. H. Kim, E. Dayalan, G. U. Sumanasekera, M. K. Sunkara, *Nano Lett.* **2012**, *12*, 1784–1788.
[27] A. Krause, S. Dorfler, M. Piwko, F. M. Wisser, T. Jaumann, E. Ahrens, L. Giebeler, H. Althues, S. Schadlich, J. Grothe, *Sci. Rep.* **2016**, *6*, 27982.
[28] I. B. Himendra Jha, X. Cui, S. Meini, H. A. Gasteiger, *J. Electrochem. Soc.* **2015**, *9*.
[29] Y. Yang, M. T. McDowell, A. Jackson, J. J. Cha, S. S. Hong, Y. Cui, *Nano Lett.* **2010**, *10*, 1486–1491.
[30] R. Dharmasena, A. K. Thapa, R. K. Hona, J. Jasinski, M. K. Sunkara, G. U. Sumanasekera, *RSC Adv.* **2018**, *8*, 11622–11632.
[31] B. K. K. Kasem, S. Jones, *Platinum Met. Rev.* **2008**, *52*, 100–106.
[32] J. Hassoun, Y.-K. Sun, B. Scrosati, *J. Power Sources* **2011**, *196*, 343–348.
[33] F. Xu, X. Li, F. Xiao, S. Xu, X. Zhang, P. He, H. Zhou, *Adv. Perform. Mater.* **2016**, *31*, 517–520.

Manuscript received: November 12, 2019
Revised manuscript received: December 19, 2019
Accepted manuscript online: December 20, 2019
Version of record online: January 16, 2020